Theor Chem Acc (2013) 132:1359
DOI 10.1007/s00214-013-1359-3

REGULAR ARTICLE

Manipulating the singlet–triplet transition in ion strings by nonresonant dynamic Stark effect

Patricia Vindel-Zandbergen · Mirjam Falge · Bo Y. Chang · Volker Engel · Ignacio R. Sola

Received: 30 October 2012 / Accepted: 7 March 2013 / Published online: 20 April 2013

Abstract Using strong laser pulses, we show that it is possible to control the spin state in a model system based on a two-electron extension with spin couplings of the Shin–Metiu Hamiltonian, truncated to account for the lowest electronic energy states. We consider two different models depending on the number of electronic states included in the calculation. The initial electronic state determines when the spin state is stable or not in the absence of an external field. In the latter case, by nonresonant dynamic Stark effect, we show that it is possible to avoid spin transitions with strong fields, using different pulse frequencies. This effective spin locking requires minimizing absorption to excited singlets as well as decoupling the singlet and triplet electronic states. In the first case, we show that it is possible to force the spin transition by a combination of two pulses, a chirped pulse and a transform limited pulse, where the time-delay must be chosen to maximize spin switching on a different electronic state. Our results show that forcing the spin switching is a more difficult goal than avoiding it and that this goal becomes highly restricted when many electronic pathways or multi-photon processes are available.

Keywords Dynamic Stark effect · Wave-packet dynamics · Quantum control

Published as part of the special collection of articles derived from the 8th Congress on Electronic Structure: Principles and Applications (ESPA 2012).

P. Vindel-Zandbergen · I. R. Sola (✉)
Departamento de Quimica Fisica, Universidad Complutense, 28040 Madrid, Spain
e-mail: ignacio@tchiko.quim.ucm.es

M. Falge · V. Engel
Institut für Physikalische und Theoretische Chemie and Röntgen Research Center for Complex Material Systems, Universität Würzburg, Campus Nord, Emil-Fischer-Str. 42, 97074 Würzburg, Germany

B. Y. Chang
School of Chemistry (BK21), Seoul National University, Seoul 151-747, Republic of Korea

1 Introduction

Laser control of quantum processes is an active arena particularly in the application of femtosecond laser pulses to quantum-state excitation and unimolecular reactions [1–3]. Successful laser control experiments have been reported in an increasing variety of physical systems, including complex chemical and biological processes [1, 2].

Addressing the dynamics of complex systems, the mechanism of the optical control is often understood from the spectral features of the pulses [4] (albeit with important caveats [5]), implying correlations between the pulse frequencies and the Hamiltonian resonances, with relative phases of the spectrum adding important dynamical information concerning the cross-talk of the resonances [6]. However, this picture is no longer valid when strong fields are used. Nonresonant effects may then completely shift or distort the Hamiltonian spectrum, which is no longer independent of the pulse spectrum [7–13]. It is possible to base the control mechanism solely on the effects of the nonresonant dynamic Stark effect (NRDSE) [14–18]. This strategy is particularly useful when the aim of the control problem is to "disconnect" an undesired transition [16, 17]. The NRDSE is behind many interesting control scenarios involving molecular alignment [19–26], the control of photodissociation reactions [14, 15, 27–29], or the control

of singlet–triplet transitions [16–18], which is also the motivation of this work.

The spin–orbit coupling is a relativistic effect that mainly affects the Hamiltonian of systems with heavy nuclei [30]. In molecules, the spin–orbit transition is one of the main sources that causes the breakdown of the Born–Oppenheimer approximation in the dynamics of excited states, inducing intersystem crossing (ISC) and altering the spectroscopy and photodissociation of molecules and the relaxation rates in complex biological systems [31, 32]. Although in not heavy atoms, the mass is often invoked as a reason to neglect the ISC processes, simulations of the dynamics of polyatomic molecules with light atoms have shown that the effect of ISC must be taken into account in many occasions [33–35]. In solids, the spin coupling between different states can be used to create states of mixed multiplicity and to prepare optical spin switches [36–39]. These are important in spintronics [40] and may have potential application as quantum information storage or quantum information processing devices [41].

Rather than using a realistic Hamiltonian for a particular system, in this work we use the very generic Shin–Metiu (SM) Hamiltonian that models charge transfer processes in some matrix environments [42–47]. The original SM model is conveniently extended to include two electron processes with singlet–triplet couplings [48, 49]. This extended Shin–Metiu (ESM) model is particularly interesting because one can treat electron and nuclear processes at the same level, without invoking the Born–Oppenheimer approximation. Recently, we have shown that in the dynamics of the ESM with strong fields, ionization is important and it is in fact the dominant process [49]. In this work, however, we neglect ionization and use the adiabatic states (electronic potential curves) obtained from the electronic Hamiltonian of the ESM in the Born–Oppenheimer approximation to simulate the dynamics of the nuclear coordinates under the influence of laser pulses and singlet–triplet couplings. For this reason, in Sect. 2 we study the ESM and give the different electronic potentials and couplings. We also show the spin-coupling dynamics of the system starting from different initial states.

The goal of the study is to survey the extent to which optical control of the singlet–triplet transfer is possible, either by adiabatically "freezing" the spin populations by means of a laser, such that the rate of spin transfer is substantially reduced, or by forcing the spin transition when this is negligible. The control of these processes is based either on a pump–dump pulse sequence or on the NRDSE scheme, whose principles are briefly reviewed for the system of study in Sect. 3. Preliminary results have shown that the NRDSE scheme can induce spin freezing, although ionization takes over the system in <50 fs. In this work, we study in detail the processes of both spin locking and spin switching. Two models of different complexity (involving different number of electronic states and couplings) are introduced. In Sect. 4, we analyze spin locking for both models, outlining the different roles of the pulse parameters, and in Sect. 5, we study the more difficult process of spin-state switching. Finally, Sect. 6 is the summary and conclusions.

2 Hamiltonian model and field-free dynamics

The electronic potentials and dipole couplings are obtained from the Born–Oppenheimer limit of an extended version of the Shin–Metiu model (ESM), including spin couplings. The ESM consists of an ion (coordinate R) and two electrons (coordinates x, y) confined to move in a single dimension, interacting with each other and two additional fixed ions through screened Coulomb interactions. Because of exchange symmetry, the spatial wave function is either symmetric ($\psi^S(x, y, R, t)$, singlet (S)) or anti-symmetric ($\psi^T(x, y, R, t)$, triplet (T)) with respect to electron exchange. Details are given in ref. [49].

The spin uncoupled Born–Oppenheimer potential energy curves and electronic wave functions are obtained by imaginary time propagation of an electronic wave function of singlet/triplet symmetry $\psi^M(x, y, t;R)$ ($M = S, T$) at fixed nuclear position R

$$\psi^M(x, y, t; R) = e^{-H_{\mathrm{el}}t}\psi^M(x, y, t = 0; R) \tag{1}$$

with the electronic Hamiltonian operator

$$H_{\mathrm{el}}(x, y, R) = -\frac{1}{2}\frac{\partial^2}{\partial x^2} - \frac{1}{2}\frac{\partial^2}{\partial y^2} + V(x, y, R) \tag{2}$$

for different values of R. In the absence of spin coupling in the electronic Hamiltonian, the wave function symmetry is conserved. For long times, t, $\psi^M(x, y, t;R)$ converges to the ground state $\varphi_1^M(x, y, R)$ of the respective symmetry and the norm of the wave function decreases as $N(t) = e^{-2V_1(R)t}$. After the ground state is determined, the next higher eigenstate $\varphi_2^M(x, y, R)$ is obtained by another imaginary time propagation starting from an initial state where the ground state is projected out:

$$\begin{aligned}\tilde{\psi}^M(x, y, t = 0; R) &= \psi^M(x, y, t \\ &= 0; R) - \left\langle \psi^M(x, y, t = 0; R) \middle| \varphi_1^M(x, y, R) \right\rangle \\ &\quad \cdot \varphi_1^M(x, y, R).\end{aligned} \tag{3}$$

Higher eigenstates are calculated successively using the same scheme. In this way, the basis of Born–Oppenheimer electronic states $\{\varphi_j^M(x, y, R)\}$ and their respective potential curves $V_j^M(R)$ are obtained. Dipole and spin couplings are evaluated with respect to these electronic basis as well.

To monitor spin transitions, we introduce in a heuristic way a spin-coupling term of the form

$$J(x,y) = \lambda(x-y), \tag{4}$$

where the coupling strength-parameter is chosen as $\lambda = 1.028 \times 10^{-3}$ eV/Å. For simplicity, we neglect the possible dependence of the coupling on the nuclear coordinate R. $J(x, y)$ creates new potential energy terms that couple (and mix) the Born–Oppenheimer electronic potentials. They are obtained from

$$V_{S_n,T_m}(R) = \int \mathrm{d}x\,\mathrm{d}y\,\varphi_n^S(x,y,R)J(x,y)\varphi_m^T(x,y,R). \tag{5}$$

where φ_n^S and φ_m^T denote the electronic eigenfunctions of singlet and triplet symmetry, respectively. To monitor laser-driven dynamics, we calculate the transition dipole moments

$$\mu_{M_n,M_m}(R) = \int \mathrm{d}x\,\mathrm{d}y\,\varphi_n^M(x,y,R)(-x-y)\varphi_m^M(x,y,R). \tag{6}$$

where $M = S$ or T.

In Fig. 1, we show the first electronic singlet and triplet potentials obtained from the ESM Hamiltonian for a particular choice of parameters (screening parameters $R_c = R_e = R_f = 1.5$ Å and charge numbers $Z_1 = Z_2 = Z = 1$ for the ESM Hamiltonian, see ref. [49]), neglecting the spin-coupling terms. The general feature of these potentials is that the singlet and triplet states come on pairs, showing either a double-well structure or a single equilibrium geometry at $R = 0$. Because the two electrons tend to be at opposite sides of the central ion (that is, each facing a different end-ion), the exchange symmetry of the electronic wave function does not lead to substantial energy differences between the singlet and the triplet wave functions. Thus, the singlet–triplet transfer due to the V_{S_j,T_j} terms (for $j = 1$, 3, etc.) is expected to be large. However, V_2^S and V_2^T (V_5^S and V_5^T as well, for higher energies) have a different structure near the equilibrium geometry and the spin-coupling mechanism is not efficient for any reasonable value of λ.

In addition to the spin coupling, nonadiabatic coupling terms could have been included. The energy separation between the singlet curves (and between the triplet curves as well) makes internal conversion processes very unlikely, as shown in the numerical results obtained solving the full vibronic Hamiltonian [49]. Thus, we neglect their contribution in the present work.

In Fig. 2, we show the population dynamics starting either from V_1^S or from V_2^S in the absence of any external field. We solve the time-dependent Schrödinger equation for the nuclear motion in two electronic states (S_j and T_j, for j either 1 or 2),

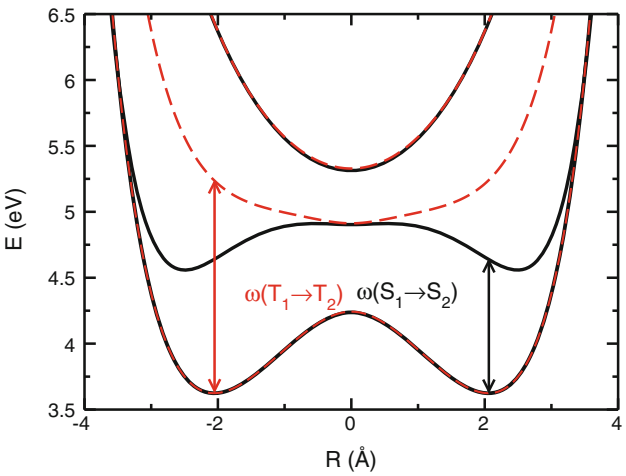

Fig. 1 Potential *curves* for the lowest three electronic states with singlet ($M = S$, *solid lines*) and triplet ($M = T$, *dashed lines*) symmetries. Notice that T_1 and T_3 practically coincide with S_1 and S_3, while S_2 and T_2 have different equilibrium geometries. Also shown in the *figure* are the frequencies for the Franck–Condon resonant transition between $S_1 \rightarrow S_2$ and $T_1 \rightarrow T_2$

$$i\frac{\partial}{\partial t}\begin{pmatrix}\psi_j^S\\ \psi_j^T\end{pmatrix} = -\frac{1}{2m}\frac{d^2}{\mathrm{d}R^2}\begin{pmatrix}\psi_j^S\\ \psi_j^T\end{pmatrix} + \begin{pmatrix}V_j^S(R) & V_{S_j,T_j}(R)\\ V_{S_j,T_j}(R) & V_j^T(R)\end{pmatrix}\begin{pmatrix}\psi_j^S\\ \psi_j^T\end{pmatrix} \tag{7}$$

using the split-operator with fast Fourier transform technique. In Eq. (7), m is the mass of a proton.

For the choice of the coupling parameter λ, we observe full singlet–triplet switching in a period $T \sim 120$ fs starting in V_1^S, and practically no triplet contamination starting from V_2^S (the maximum population in T_2 is 3×10^{-5}). The goal of this work is to design optical processes to avoid the spin

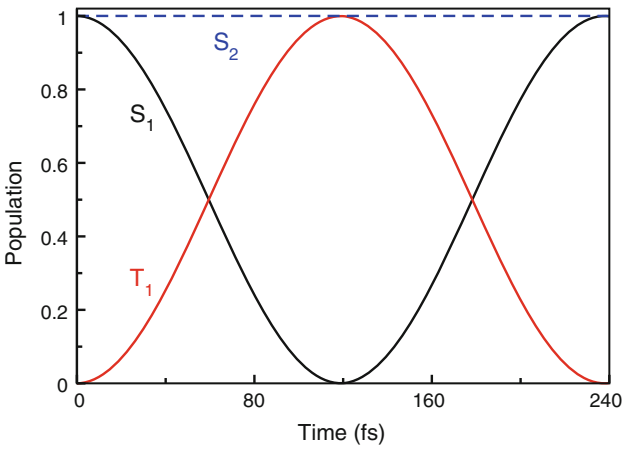

Fig. 2 Singlet triplet population transfer in the absence of an external field. In *solid lines*, we show the population of S_1 and T_1 when the dynamics starts in S_1. In *dashed line,* we show the population of S_2 when the dynamics starts from this excited state. In this case, the population in T_2 remains practically zero and it is not shown

dynamics from V_1^S (that is, to induce *spin locking*) and to force it starting from V_2^S (that is, to induce *spin switching*). To that end, we will use the NRDSE or a pump–dump scheme.

3 The NRDSE scheme

In order to understand the physical mechanism underlying the control of the spin coupling via the NRDSE, it is enough to consider the simplest polarizable two-level system with one singlet (S) and one triplet (T) state, coupled via V_{ST}, whose energy can be Stark shifted by a nonresonant electromagnetic field with envelope $\mathcal{E}(t)$ [50]. Suppose that for a given field frequency, the dynamic polarizabilities for the singlet and triplet states are $\alpha_j(\omega)$ ($j = S, T$, we will often omit the frequency dependence in the following). Then choosing the field-free singlet energy as the zero point of energy, the effective Hamiltonian for the system is

$$\mathsf{H} = \begin{pmatrix} -\alpha_S \mathcal{E}(t)^2/2 & V_{ST} \\ V_{ST} & \Delta(0) - \alpha_T \mathcal{E}(t)^2/2 \end{pmatrix} \tag{8}$$

where $\Delta(0)$ is the energy difference between the states in the absence of the field. One can choose an instantaneous zero point of energy that includes the Stark-shift contribution to the singlet energy, making the Hamiltonian

$$\mathsf{H} = \begin{pmatrix} 0 & V_{ST} \\ V_{ST} & \Delta(\mathcal{E}) \end{pmatrix} \tag{9}$$

where $\Delta(\mathcal{E}) = \Delta(0) - (\alpha_T - \alpha_S)\mathcal{E}^2(t)/2$. The Rabi formula can then be used to predict the spin-coupling dynamics. Suppose the system is initially in the singlet state, assuming for simplicity a constant envelope $\mathcal{E}$, the population in the triplet will be

$$P_T = \left(\frac{V_{ST}}{\Omega_e}\right)^2 \sin^2 \Omega_e t \tag{10}$$

where $\Omega_e = \sqrt{V_{ST}^2 + \Delta(\mathcal{E})^2}$. For instance, if $\Delta(0) \ll |V_{ST}|$ (as in the ESM model, starting in V_1^S where $\Delta(0) = 0$), substantial spin transfer will occur at $\tau_{ST} = \pi / 2V_{ST}$. This spin-mixing dynamics can be halted while a laser pulse acts if $\Delta(\mathcal{E}) \gg V_{ST}$. Conversely, if $\Delta(0) \gg V_{ST}$ (as in the ESM starting in V_2^S) full population transfer can be induced by making $\Delta(\mathcal{E}) = 0$ and timing the pulse duration exactly as $\tau_e = \pi/2\Omega_e$. Thus, a laser-controlled spin switch can be created whenever the dynamic polarizability of the singlet state is different from that of the triplet state, $\alpha_S \neq \alpha_T$. Moreover, the dynamic polarizabilities depend on the pulse frequency ω as well. Additionally, the two-level theory can be used to propose alternative (more robust) quantum control scenarios [50].

The extension of the effective 2-level Hamiltonian to the nuclear Hamiltonian in the Born–Oppenheimer approximation is straightforward. Neglecting population absorption one can obtain [51]

$$\mathsf{H} = -\frac{1}{2m}\frac{d^2}{dR^2}\mathsf{I} + \begin{pmatrix} V_1^S(R) - \alpha_S(R,\omega)\mathcal{E}(t)^2/2 & V_{S_1,T_1}(R) \\ V_{S_1,T_1}(R) & V_1^T(R) - \alpha_T(R,\omega)\mathcal{E}(t)^2/2 \end{pmatrix} \tag{11}$$

Since $V_{S_1,T_1}(R)$ is almost constant (and small) around the equilibrium geometries of the V_1^S potential and $V_1^S(R) \approx V_1^T(R)$, in the absence of the field, the population dynamics is practically that of a two-level system, where the singlet–triplet population transfer does not lead to wave-packet dynamics. This prediction explains the excellent agreement between the population dynamics in Fig. 2 and the result of applying the Rabi formula. For strong fields, however, Eq. (11) does not give quantitative results. Firstly, because it is difficult to evaluate the dynamic polarizabilities $\alpha_j(R, \omega)$, and secondly, because multi-photon absorption to excited states usually cannot be neglected. Therefore, in the following results, we solve the time-dependent Schrödinger equation including different sets of electronic states.

Within the Born–Oppenheimer approximation, the nuclear dynamics Hamiltonian in the presence of the control field $\epsilon_c(t)$, is

$$\mathsf{H}^{\text{eff}} = -\frac{1}{2m}\frac{\mathrm{d}^2}{dR^2}\mathsf{I} + \begin{pmatrix} V_1^S & -\mu_{S_1,S_2}\epsilon_c(t) & V_{S_1,T_1} & V_{S_1,T_2} \\ -\mu_{S_1,S_2}\epsilon_c(t) & V_2^S & V_{S_2,T_1} & V_{S_2,T_2} \\ V_{T_1,S_1} & V_{T_1,S_2} & V_1^T & -\mu_{T_1,T_2}\epsilon_c(t) \\ V_{T_2,S_1} & V_{T_2,S_2} & -\mu_{T_1,T_2}\epsilon_c(t) & V_2^T \end{pmatrix} \tag{12}$$

where I is the 4×4 unit matrix. In Eq. (12), we have restricted the Born–Oppenheimer expansion to the minimal symmetric set (MSS) of electronic states that can represent the dynamics of the system under the influence of an external field that controls the singlet–triplet transition. In the numerical calculations, we use "square" laser pulses with fast ramps of $\sin^2(\pi(t - t_0)/\tau_s)$ form. The switching on/off time is set to $\tau_s = 25$ fs.

The extension of the model to include a more complete set of electronic states is straightforward. In addition to the MSS, we have considered a model including the 6 lowest singlet and triplet states (LSS). These 12 Born–Oppenheimer states span the energy range of any 3-photon process starting in S_1 for all laser frequencies used in this work. It should be noted though that the ESM model favors fast multi-photon excitation from the initial state to the ionization continuum [49]. The ionization process is not considered in this work. However, as pointed out in [49], the ionization process does not affect considerably the spin

dynamics and some observables such as the averaged spin angular momentum of the system, hint that the controlled process is still acting on the small population surviving ionization.

4 Spin-state locking

4.1 Dynamics using the MSS model

The results with the MSS model can be used as proof-of-principles for the optical control of the singlet–triplet transition. The initial state is the ground vibrational eigenstate of S_1, which is an even function with maximum probability on both potential wells. As an example, in Fig. 3, we show the population dynamics in the four electronic states using a single control pulse ϵ_c with different parameters that give best results over different frequency intervals. The overall duration of the pulse is set to 200 fs to display more clearly the effect of spin locking.

We have found robust solutions in the space of parameters for a broad range of peak intensities and frequencies. Although strong pulses are needed to overcome the small transition dipole, the results are not very sensitive to the peak intensity. In general, for larger peak amplitude ϵ_0 the

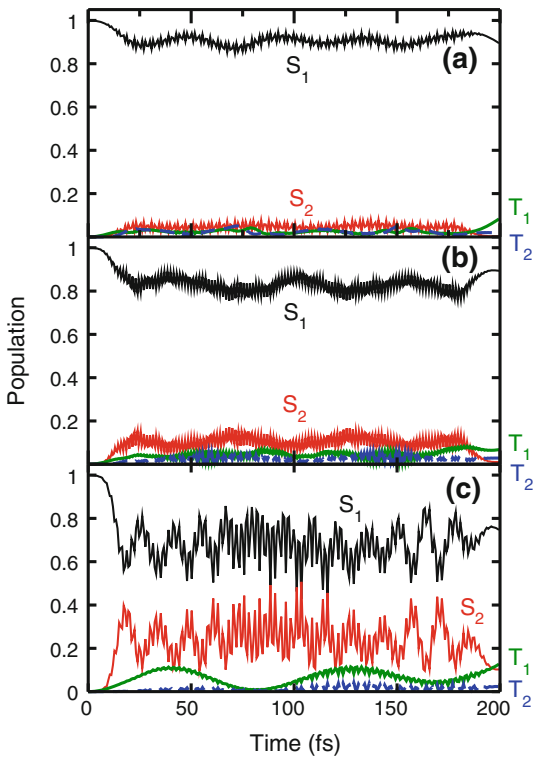

Fig. 3 Electronic states population dynamics in the MSS model with different pulse frequencies and intensities: **a** with $\hbar\omega = 1.63$ eV and $I_0 = 10.1$ TW/cm^2, **b** with $\hbar\omega = 1.41$ eV and $I_0 = 10.1$ TW/cm^2 and **c** with $\hbar\omega = 0.87$ eV and $I_0 = 8.95$ TW/cm^2

population is more evenly spread between the singlet potentials with smaller excitation of the triplet states.

The frequency must be chosen detuned from the $S_1 \rightarrow S_2$ resonance ($\hbar\omega(S_1 \rightarrow S_2) \approx 1$ eV), defined in the initial Franck–Condon region, to avoid absorption to a different state. In the example of Fig. 3a, $\hbar\omega = 1.68$ eV is slightly above the resonance between T_1 and T_2 ($\hbar\omega(T_1 \rightarrow T_2) \approx 1.6$ eV) and thus clearly blue shifted with respect to $\omega(S_1 \rightarrow S_2)$. Therefore, we expect a larger positive Stark-shift on V_1^T than in V_1^S, allowing the effective decoupling of these potentials with $\epsilon_0 = 0.017$ a.u. or larger (implying a peak intensity I_0 of 10.1 TW/cm^2).

Other frequency intervals can be chosen: If ω is between $\omega(S_1 \rightarrow S_2)$ and $\omega(T_1 \rightarrow T_2)$ the dynamic Stark-shift should be positive in V_2^S but negative in V_1^T. Weaker fields could then decouple the electronic states. However, it is more difficult to avoid populating the V_2^S potential. For the results in Fig. 3b, we use $\hbar\omega = 1.39$ eV and the same peak intensity ($I_0 = 10.1$ TW/cm^2).

With $\omega < (\omega(S_1 \rightarrow S_2), \omega(T_1 \rightarrow T_2))$ both V_2^S and V_1^T experience a negative Stark-shift (larger in V_1^S) that give similar results as those shown in case (a). However, multi-photon excitation to S_2 becomes resonant and as a result, more population is excited to S_2. The different shapes of the potentials induce nuclear motion that shows up in some Rabi oscillations between the electronic populations in S_1 and S_2. In Fig. 3c, for $\hbar\omega = 0.84$ eV, we have slightly reduced the pulse intensity to $I_0 = 8.95$ TW/cm^2.

4.2 Dynamics in the LSS model

When considering a larger set of electronic states, the control of the process becomes more complex. On one hand, the different electronic states normally *add* to the polarizabilities, increasing the effect of the Stark effect: weaker pulses could in principle be used. On the other hand, one has to care about many possible resonances ($\omega(S_1 \rightarrow S_j), \omega(S_j \rightarrow S_k)$) that lead to absorption and multi-photon ladder climbing of electronic states. Given the intensities required to decouple the singlet–triplet transition, the second effect is clearly more dominant than the first one, making the spin-state locking quite more challenging in the LSS model than in the MSS model.

In Fig. 4, we analyze the time-averaged populations in the triplets and excited singlets (all except S_1) as a function of the pulse frequency and intensity

$$\langle P_T \rangle = \frac{1}{\tau_l} \sum_{j=1}^{6} \int_0^{\tau_l} \left\langle \psi_j^T(t) | \psi_j^T(t) \right\rangle \mathrm{d}t$$
$$\langle P_{ES} \rangle = \frac{1}{\tau_l} \sum_{j>1}^{6} \int_0^{\tau_l} \left\langle \psi_j^S(t) | \psi_j^S(t) \right\rangle \mathrm{d}t \qquad (13)$$

where $\tau_l = 200$ fs is the pulse duration. The goal of decoupling the $S_1 \rightarrow T_1$ transition involves minimizing $\langle P_T \rangle$ (avoiding the singlet–triplet transition) and $\langle P_{ES} \rangle$ (avoiding the absorption to other electronic states). Whereas with stronger pulses, $\langle P_T \rangle$ is small for all the range of frequencies explored in this work, $\langle P_{ES} \rangle$ is particularly large at lower frequencies, obviously around $\omega(S_1 \rightarrow S_2)$, but also very much until $\omega > \omega(T_1 \rightarrow T_2)$. Disregarding vibrational excitation, the LSS model includes all singlet states that can be accessed by three photons at $\hbar\omega \sim 1.7$ eV.

In Fig. 5, we show the population dynamics for three different cases. For the three frequency windows $\omega < \omega(S_1 \rightarrow S_2)$ (smaller), $\omega(S_1 \rightarrow S_2) \leq \omega \leq \omega(T_1 \rightarrow T_2)$ (intermediate) and $\omega > \omega(T_1 \rightarrow T_2)$ (larger), we have chosen ω and ϵ_0 such that both $\langle P_T \rangle$ and $\langle P_{ES} \rangle$ are minimized. This gives $\hbar\omega = 0.87$ eV, $I_0 = 7.9$ TW/cm^2; $\hbar\omega = 1.41$ eV, $I_0 = 5.0$ TW/cm^2; and $\hbar\omega = 1.63$ eV, $I_0 = 10.1$ TW/cm^2, respectively.

In general, for all frequencies below the $S_1 \rightarrow S_2$ resonance at the pulse intensities needed for spin locking, there is always substantial absorption to excited singlet states. For the best results shown in Fig. 5, the population in the singlets is mostly steady at 0.9 (although there is some slow decay into the triplets) but the population is widely spread between S_1, S_2 and S_3. The ladder climbing excitation mechanism is very efficient in the ESM model.

As discussed in Sect. 3, the NRDSE mechanism is more efficient using intermediate frequencies. Thus, spin locking can be achieved with less intense pulses. To minimize absorption to S_3, the frequency must be smaller than 1.42 eV. However, 3-photon excitation to S_5 cannot be avoided. In the best results shown in Fig. 5, 90 % of the population is kept on the singlet states, but there is a clear beating between population in S_1 and S_5. Within the constraints of the LSS model, best results are obtained for larger frequencies. Here, part of the population goes to S_6.

In Fig. 6, we show the evolution of the nuclear probability density of all the singlet states for smaller and intermediate frequencies (the results for larger frequencies are very similar to those for intermediate frequencies). In the first case, the nuclear wave packet spreads and becomes mostly delocalized (although some coherent vibrational motion can be observed). This is mainly because the geometry of S_3 (with a single minima) is very different from that of S_1 and S_2. Surprisingly, very little singlet–triplet transfer is observed in the population of the different excited singlet states. When the laser is turned off only a small fraction of the population undergoes singlet–triplet conversion.

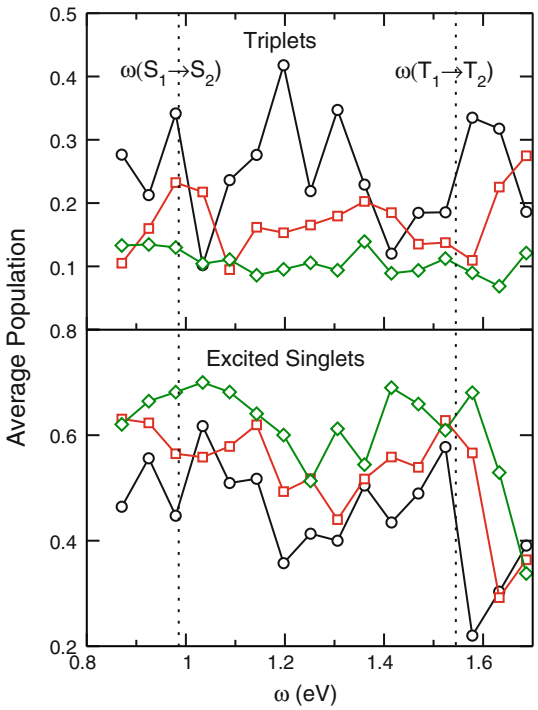

Fig. 4 Time-averaged population in all the triplet and all excited singlet states as a function of pulse frequency and intensity, for peak intensities (in TW/cm^2) of 5.0 (*circles*), 7.9 (*squares*) and 10.1 (*diamonds*). The vertical lines represent the frequencies at which the $S_1 \rightarrow S_2$ and $T_1 \rightarrow T_2$ Franck–Condon transitions are resonant at the equilibrium geometry

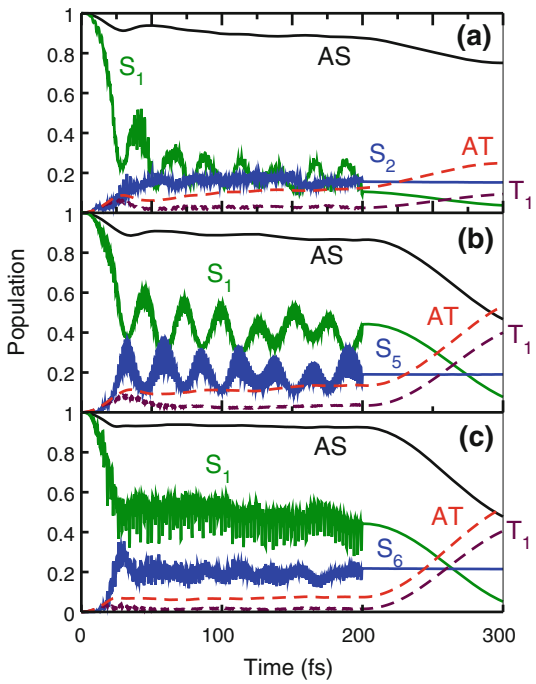

Fig. 5 Electronic states population dynamics in the LSS model with best pulse parameters in the three frequencies ranges. **a** with $\hbar\omega = 0.87$ eV $< \hbar\omega(S_1 \rightarrow S_2)$, **b** with $\hbar\omega(S_1 \rightarrow S_2) \leq \hbar\omega = 1.41$ eV $\leq \hbar\omega(T_1 \rightarrow T_2)$ and **c** with $\hbar\omega = 1.63$ eV $> \hbar\omega(T_1 \rightarrow T_2)$. Other parameters are given in the text. *AS* stands for the population of all singlet states and *AT* for the population of all the triplet states

For intermediate and larger frequencies, the nuclear wave-packet dynamics is still mostly confined to the bottom of the potential energy in V_1^S and much singlet–triplet conversion is observed when the laser is turned off.

5 Spin-state switching dynamics

As discussed in Sect. 2, almost all electronic singlet states practically overlap with the triplet states, so that the spin-transfer dynamics is very efficient. For the lowest energy potentials, only in S_2, there is no singlet–triplet transition. Following the NRDSE recipe (Sect. 3), in order to transfer the population from S_2 to T_2, one first needs to force a near-degeneracy of the two electronic states by Stark shifting the states using a strong nonresonant pulse. The electronic structure of the singlets around S_2 is quite different from that of the triplets around T_2 (S_2 is closer to S_1 while T_2 is closer to T_3), so that in principle the dynamic polarizabilities can be quite different and the NRDSE can be applied. However, the energy difference between the states at the equilibrium configuration of S_2 is approximately 1 eV, while the transition electronic dipoles are relatively small, making it impossible to compensate the energy difference by Stark-shift using any reasonably strong laser pulse. Thus, the singlet–triplet transfer cannot be indirectly induced by a single control pulse.

Instead of applying the NRDSE, in this work, we design an alternative dump–pump strategy that requires two pulses controlling the time-delay between them. The idea is sketched in Fig. 7. First, we apply a dump pulse that moves the population from S_2 to S_1. Then, we wait for the efficient singlet–triplet transfer between S_1 and T_1. Finally, a pump pulse is applied to transfer the population from T_1 to T_2. In the following, we present the results obtained within the MSS model.

A typical result with approximately optimized pulse parameters is shown in Fig. 8. Here, we have chosen a negatively first chirped pulse with intensity $I_0 = 5.9$ TW/cm^2, duration $\tau_l = 90$ fs and frequency $\omega(t) = \omega_0 + \beta (t - t_0)/2$, where $\hbar\omega_0 = 1.15$ eV, $\hbar\beta = -0.0136$ eV/fs and t_0 is the center of the pulse. The transformed-limited second pulse has $I_0 = 0.9$ TW/cm^2, $\tau_l = 40$ fs and $\hbar\omega_0 = 1.52$ eV. The parameters of the first pulse are optimized to achieve maximal population transfer (approx 90 %) in a reasonably short time. Since the equilibrium geometry of S_2 and S_1 is very similar, it is difficult to disentangle the optical Rabi flopping between S_2 and S_1 from the spin Rabi flopping between S_1 and T_1. To avoid the $S_1 \rightarrow S_2$ back-transition, one needs to use chirped pulses. We chose a negative chirp, but it is possible to use positively chirped pulses as well. Since the $S_2 \rightarrow S_1$ Franck–Condon transition is at lower energies than the $S_2 \rightarrow S_3$ transition, at first look the choice of a positive chirp would seem a better option to minimize absorption into highly excited singlet states. For the MSS model, however, the results are slightly better for the negatively chirped pulses.

On the other hand, the equilibrium geometry of T_1 is very different from that of T_2. The time-delay between the pulses, $\tau_d = 110$ fs, is chosen to facilitate maximal singlet–triplet conversion between S_1 and T_1. For the second pulse, one can use a transformed-limited pulse because the wave packet in T_2 moves away from the Franck–Condon window and naturally deactivates the probability of stimulated emission. The parameters of the second pulse are chosen to maximize the yield of the $T_1 \rightarrow T_2$ transition in a very short time.

In Fig. 9, we show a contour plot of the time evolution of the nuclear probability densities of singlet and triplet spin character, separately. During the $S_2 \rightarrow S_1$ stimulated

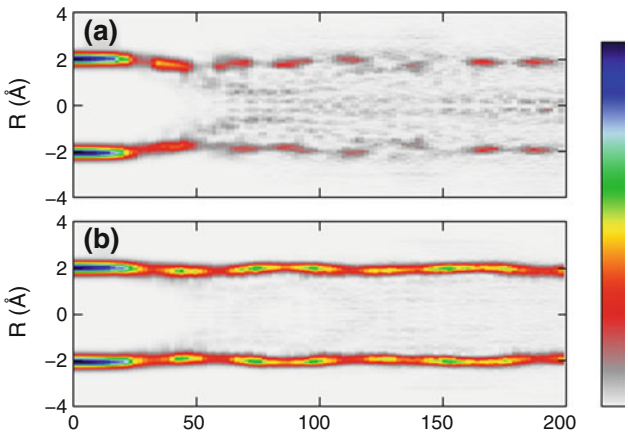

Fig. 6 Nuclear probability density for all the singlet states in the LSS model with **a** $\hbar\omega = 0.87$ eV and $I_0 = 7.9$ TW/cm^2 and **b** $\hbar\omega = 1.41$ eV and $I_0 = 5.0$ TW/cm^2

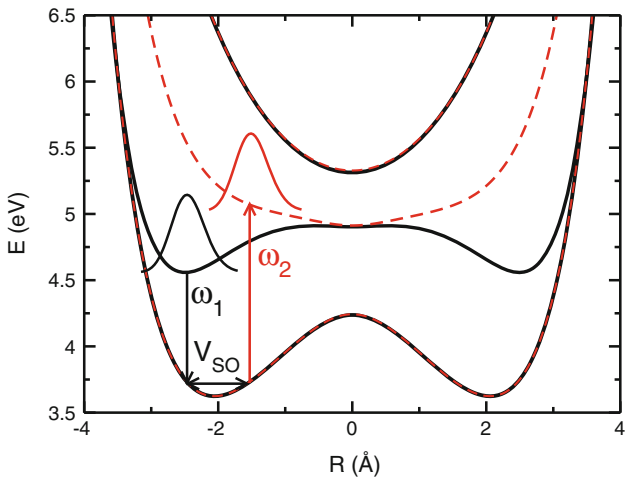

Fig. 7 Scheme of the dump–pump strategy used to induce spin switching between S_2 and T_2. We show the potential energy *curves* and the wave packets after the different stages of the process

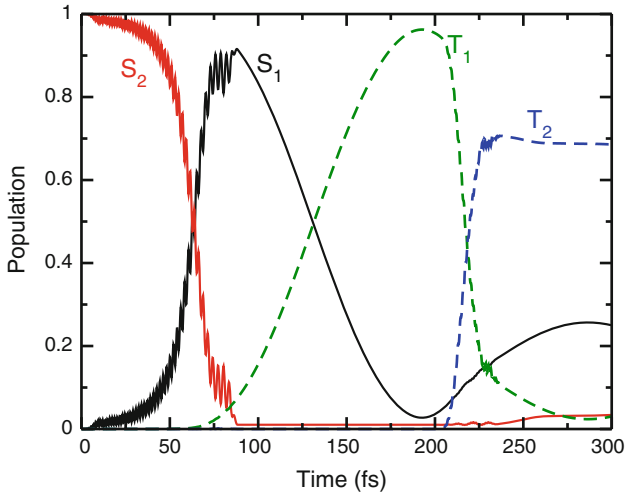

Fig. 8 Electronic states population dynamics in the MSS model applying the dump–pump scheme to induce singlet–triplet transfer from S_2 to T_2. The pulse parameters are given in the text

emission and the $S_1 \rightarrow T_1$ spin transfer, the singlet nuclear wave packet remains basically in the same region (around $R = \pm 2.5$ Å). The triplet nuclear wave packet appears at later states and moves toward $R = 0$, where the minima of T_2 is located.

Unfortunately, it is not possible to achieve similar results with the LSS model, regardless of the sign of chirp. The main problem is that in the Franck–Condon region the transition dipole between S_1 and S_2 is much smaller (a factor of 100 times smaller) than the transition dipole between S_2 and S_3 or between S_1 and S_5 or S_6. As a consequence, the dump pulse must be very strong and the transition competes with two- and three-photon absorption to other excited states, similarly at what happened when using low frequencies to lock the population in S_1. For the optimal parameters used above, a population of only 0.06

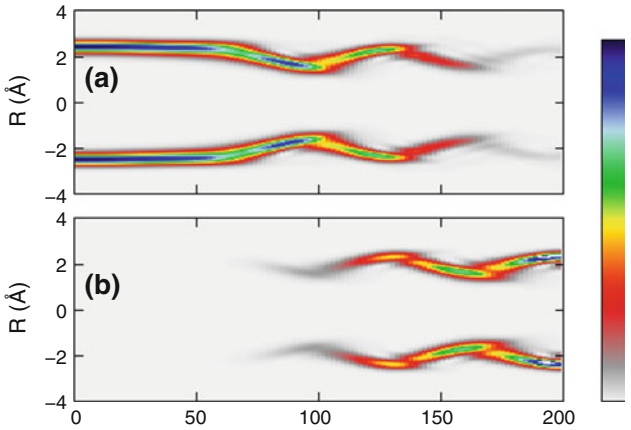

Fig. 9 Nuclear probability density in the spin-switching process for **a** all the singlet and **b** all the triplet states. The laser parameters are given in the text

arrives to T_2 at the end of the process, while singlet–triplet transitions between several excited states account for a total 22 % of population in the triplet states.

6 Summary and conclusions

In this work, we analyzed in detail the role of different laser parameters in the control of the singlet–triplet transition by means of the NRDSE. Following previous work [49], we used the ESM model to obtain the electronic potentials, dipole couplings and singlet–triplet couplings. Depending on the number of potentials included in the calculation, we defined two approximate models: the minimal MSS model and the larger LSS model. Multiphoton ionization and internal conversion were not taken into account. The time-dependent Schrödinger equation for the nuclear motion was then solved for these models starting from different electronic states in order to force spin locking when the laser-free dynamics implied full singlet-triplet conversion, or spin switching, when the laser-free dynamics conserved the spin state.

Certainly, the 3-D 5-particle collinear ESM Hamiltonian implies strong restrictions on the motion of the electrons and ion which show in the potentials and couplings. In particular, the singlet and triplet electronic states tend to have very similar energies, facilitating fast ISC processes. On the other hand, the model favors multiphoton ladder-type ionization, making strong-field control rather difficult. Still, we believe that the ESM is sufficiently flexible to allow the interplay of very different processes which can be analyzed to great detail, making the model an excellent numerical "laboratory" to test different control scenarios.

In this work, we focused on finding appropriate laser strategies and tuning the laser parameters in conditions where there is strong competence between different nonlinear processes, albeit disregarding ionization. Although appropriate laser parameters for spin switching were difficult to find even in the MSS model and were not found in the LSS model, spin locking was shown to be possible for different frequency windows. The smallness of the dipole couplings in the Franck–Condon region required the use of very strong pulses, which drove population to excited singlet states and thus opened new routes for spin transitions from the excited singlet to excited triplet states. Forcing a balance between two goals, minimizing the population in the triplet states and the population in the excited singlet states, was found to be a good strategy to identify control pulse frequencies and intensities that would maximally decouple the initial singlet state from the triplet states while at the same time they minimize the disturbance on the system.

Although previous work [49] showed that multi-photon ionization is the fastest process in the ESM model under the pulse intensities used in this work, the results also showed that ionization occurred mainly in the Franck–Condon window and did not affect the spin dynamics. In particular, the NRDSE was shown to maintain the control on the spin populations of the remaining (nonionized) parts of the system. Given that the full vibronic dynamics requires considerable computation time, the strategy used in this work also paves the way to identifying the best control scenarios when ionization is taken into account. We expect that this control strategy will be effective when the required laser intensity is smaller, for instance in weaker spin-coupling conditions.

Acknowledgments We thank Manfred Lein for general discussions at different stages of this work. I. R. S. and P. V. acknowledge support from the Dirección General de Investigación of Spain under Project No. CTQ2008-06760. B. Y. C. thanks the Basic Science Research Program by the National Research Foundation of Korea grant (2010-0005643). M. F. and V. E. acknowledge financial support by the State of Bavaria (Bayerisches Eliteförderungsgesetz) and by the DFG within the FOR1809. This project was supported by the COST-action CM0702 (Chemistry with Ultrashort Pulses and Free-Electron Lasers).

References

1. Rice SA, Zhao M (2000) Optical control of molecular dynamics. Wiley-Interscience, New York
2. Brixner T, Pfeifer T, Gerber G, Wollenhaupt M, Baumert T (2005) Chap 9: Optimal control of atomic, molecular and electron dynamics with tailored femtosecond laser pulses. In: Hannaford P (ed) Femtosecond laser spectroscopy. Springer, New York, pp 225–266
3. Brumer P, Shapiro M (2012) Quantum control of molecular processes. Wiley-VCH, New York
4. Silberberg Y (2009) Quantum coherent control for nonlinear spectroscopy and microscopy. Annu Rev Phys Chem 60:277–292
5. Geremia GM, Zhu W, Rabitz H (2000) Incorporating physical implementation concerns into closed loop quantum control experiments. J Chem Phys 113:10841–10848
6. Brixner T, Kiefer B, Gerber G (2001) Problem complexity in femtosecond quantum control. Chem Phys 267:241–246
7. Bartels R, Backus S, Zeek E, Misoguti L, Vdovin G, Christov IP, Murnane MM, Kapteyn HC (2000) Shaped-pulse optimization of coherent emission of high-harmonic soft X-rays. Nature 406:164–166
8. Levis RJ, Menkir GM, Rabitz H (2001) Selective bond dissociation and rearrangement with optimally tailored strong-field laser pulses. Science 292:709–713
9. Yuan JM, George TF (1978) Semiclassical theory of unimolecular dissociation induced by a laser field. J Chem Phys 68:3040–3052
10. Bandrauk AD, Sink ML (1981) Photodissociation in intense laser fields: predissociation analogy. J Chem Phys 74:1110–1117
11. Allendorf SW, Szoke A (1991) High-intensity multiphoton ionization of H_2. Phys Rev A 44:518–534
12. Guisti-Suzor A, Mies FH, DiMauro LF, Charron E, Yang B (1995) Dynamics of H^{2+} in intense laser fields. J Phys B 28:309–339
13. Frasinski LJ, Posthumus JH, Plumridge J, Codling K, Taday PF, Langley AJ (1999) Manipulation of bond hardening in H_2^+ by chirping of intense femtosecond laser pulses. Phys Rev Lett 83:3625–3628
14. Sussman BJ, Ivanov MY, Stolow A (2005) Nonperturbative quantum control via the nonresonant dynamic Stark effect. Phys Rev A 71:051401(R)
15. Sussman BJ, Townsend D, Ivanov MY, Stolow A (2006) Dynamic Stark control of photochemical processes. Science 314:278–281
16. González-Vázquez J, Sola IR, Santamaria J, Malinovsky VS (2006) Quantum control of spinorbit coupling by dynamic Stark-shifts induced by laser fields. Chem Phys Lett 431:231–235
17. González-Vázquez J, Sola IR, Santamaria J, Malinovsky VS (2006) Optical control of the singlet–triplet transition in Rb2. J Chem Phys 125:124315
18. González-Vázquez J, Sola IR, Santamaria J, Malinovsky VS (2007) Vibrationally state-selective spinorbit transfer with strong nonresonant pulses. J Phys Chem A 111:2670–2678
19. Friedrich B, Herschbach D (1995) alignment and trapping of molecules in intense laser fields. Phys Rev Lett 74:4623–4626
20. Seideman T (1995) Rotational excitation and molecular alignment in intense laser fields. J Chem Phys 103:7887–7896
21. Ortigoso J, Rodriguez M, Gupta M, Friedrich B (1999) Time evolution of pendular states created by the interaction of molecular polarizability with a pulsed nonresonant laser field. J Chem Phys 110:3870–3875
22. Stapelfeldt H, Seideman T (2003) Colloquium: aligning molecules with strong laser pulses. Rev Mod Phys 75:543–557
23. Leibscher M, Averbukh IS, Rabitz H (2003) Molecular alignment by trains of short laser pulses. Phys Rev Lett 90:2130011–2130014
24. Suzuki T, Sugawara Y, Minemoto S, Sakai H (2008) Optimal control of nonadiabatic alignment of rotationally cold N_2 molecules with the feedback of degree of alignment. Phys Rev Lett 100:033603
25. Bisgaard CZ, Clarkin OJ, Wu GR, Lee AMD, Gessner O, Hayden CC, Stolow A (2009) Time-resolved molecular frame dynamics of fixed-in-space CS2 molecules. Science 323:1464–1468
26. Sussman BJ, Underwood JG, Lausten R, Ivanov MY, Stolow A (2006) Quantum control via the dynamic Stark effect: application to switched rotational wave packets and molecular axis alignment. Phys Rev A 73:053403
27. Chang BY, Choi H, Shin S, Lee S, Sola IR (2009) Ultrafast photodissociation assisted by strong nonresonant Stark effect: the straddling control pulse. J Mod Opt 56:811–821
28. Chang BY, Shin S, Santamaria J, Sola IR (2009) Bond breaking in light-induced potentials. J Chem Phys 130:124320
29. Chang BY, Shin S, Sola IR (2009) Further aspects on the control of photodissociation in light-induced potentials. J Chem Phys 131:204314
30. McQuarrie DA, Simon JD (1997) Physical chemistry. University Science Books, Sausalito
31. Hare PM, Crespo-Hernández CE, Kohler B (2007) Internal conversion to the electronic ground state occurs via two distinct pathways for pyrimidine bases in aqueous solution. Proc Natl Acad Sci USA 104:435–440
32. Kwo WM, Ma C, Phillips DL (2008) A doorway state leads to photostability or triplet photodamage in thymine DNA. J Am Chem Soc 130:5131–5139
33. Etinski M, Fleig T, Marian CM (2009) Intersystem crossing and characterization of dark states in the pyrimidine nucleobases uracil, thymine, and 1-methylthymine. J Phys Chem A 113:11809–11816
34. Parker DSN, Minns RS, Penfold TJ, Worth GA, Fielding HH (2009) Ultrafast dynamics of the S1 excited state of benzene. Chem Phys Lett 469:43

35. Richter M, Marquetand P, González-Vázquez J, Sola I, González L (2012) Femtosecond intersystem crossing in the DNA nucleobase cytosine. J Phys Chem Lett 3:3090
36. Gómez-Abal R, Hübner W (2002) Simple model for laser-induced electron dynamics. Phys Rev B 65:195114
37. Gómez-Abal R, Hübner W (2003) The role of spinorbit coupling in optically induced ultrafast magnetic dynamics. J Phys Condens Mater 15:S709–S722
38. Gómez-Abal R, Ney O, Satitkovitchai K, Hübner W (2004) All-optical subpicosecond magnetic switching in NiO(001). Phys Rev Lett 92:227402
39. Satitkovitchai K, Pavlyukh Y, Hübner W (2005) Ab initio study of spin–orbit coupling effects on the low-lying excited states of NiO. Phys Rev B 72:045116
40. Zutic I, Das Sarma S (2004) Spintronics: fundamentals and applications. Rev Mod Phys 76:323–410
41. Bouwmeester D, Ekert A, Zeilinger A (2000) The physics of quantum information. Springer, New York
42. Shin S, Metiu H (1995) Nonadiabatic effects on the charge transfer rate constant: a numerical study of a simple model system. J Chem Phys 102:9285–9295
43. Shin S, Metiu H (1996) Multiple time scale quantum wavepacket propagation:electro nnuclear dynamics. J Phys Chem 100:7867–7872
44. Erdmann M, Marquetand P, Engel V (2003) Combined electronic and nuclear dynamics in a simple model system. J Chem Phys 119:672–679
45. Erdmann M, Engel V (2004) Combined electronic and nuclear dynamics in a simple model system II spectroscopic transitions. J Chem Phys 120:158
46. Erdmann M, Baumann S, Gräfe S, Engel V (2004) Electronic predissociation: a model study. Eur Phys J D 30:327–333
47. Gräfe S, Engel V (2006) Local control theory applied to coupled electronic and nuclear motion. Chem Phys 329:118
48. Erdmann M, Gross EKU, Engel V (2004) Time-dependent electron localization functions for coupled nuclear-electronic motion. J Chem Phys 121:9666–9670
49. Falge M, Engel V, Lein M, Vindel-Zandbergen P, Chang BY, Sola IR (2012) Quantum wave-packet dynamics in spin-coupled vibronic states. J Phys Chem A 116:11427. doi:10.1021/jp306566x
50. Sola IR, González-Vázquez J, Malinovsky VS (2006) Optical control of a spin switch in the weak spin–orbit coupling limit. Phys Rev A 74:043418
51. Sussman BJ (2011) Five ways to the nonresonant dynamic Stark effect. Am J Phys 79:477–484